

Artykuł naukowy

## **EGMS technology for building condition assessment and disaster prevention**

Technologia EGMS w ocenie stanu budynków i zapobieganiu  
katastrofom

**Beata Wieczorek**

University of Warmia and Mazury in Olsztyn, Faculty of Geoengineering,  
Institute of Geodesy and Civil Engineering, Department of Geoinformation and Cartography,  
Oczapowskiego St. 2, 10-719 Olsztyn, Poland

### ***Abstract***

*This study investigates the application of the European Ground Motion Service (EGMS) technology in assessing technical building conditions and preventing structural disasters, focusing on Olsztyn, Poland, from 2019 to 2023. Using EGMS satellite data, the study developed a risk assessment model to identify buildings vulnerable to damage due to structural instability caused by anthropogenic or natural factors; the specific influences were not investigated. The analysis in Olsztyn, covering 14,383 buildings, reveals significant displacement variations. Damaged buildings exhibit the highest velocity movements, up from  $-7.3$  mm/year to  $+18$  mm/year vertically and from  $-12.3$  mm/year to  $+21.2$  mm/year horizontally. High values indicate a significant influence of factors such as unstable ground, structural damage or environmental impact (e.g., landslides, vibrations), which increases the risk of further damage to these buildings. In contrast, in-use (98.04% of buildings) and inactive (0.92%) buildings are more stable, with displacements typically within  $\pm 3$  mm/year. Of the buildings analyzed, 9 were classified as high risk and 56 as medium risk. Validation using historical disaster records from Olsztyn during the study period confirms the effectiveness of EGMS in enhancing risk prediction accuracy. The findings underscore EGMS's potential as a vital tool for systematic monitoring, facilitating early hazard detection, and enhancing urban safety and infrastructure resilience through data-driven disaster prevention strategies.*

**Keywords:** building disaster, displacement, European Ground Motion Service, mean velocity

**Słowa kluczowe:** katastrofa budowlana, przemieszczenie, Europejska Usługa Monitorowania Ruchów Ziemi, średnia prędkość

## Introduction

Infrastructure is exposed to both natural and anthropogenic factors, which can affect the stability of their foundations and increase the risk of structural damage. Ensuring urban safety relies on infrastructure resilience, early hazard detection, and the prevention of building disasters. Monitoring structural stability, managing risks, and minimizing potential damages require precise measurements and appropriate preventive actions. Monitoring movements and deformations of infrastructure is typically conducted on a regional or local scale, where precise measurement methods can be tailored to the specific terrain. At the local level, particular attention is given to critical structures such as bridges, roads, tunnels, and buildings. This involves using traditional geodetic techniques and modern technologies, including GPS sensors, Light Detection and Ranging (LIDAR), and Interferometric Synthetic Aperture Radar (InSAR). Early detection of hazardous displacements helps prevent building disasters.

In Poland, building disasters have been recorded since 1995. Since 2008, these data have been collected in an electronic register maintained by county and provincial building inspection authorities. This register contains information on construction objects and the causes of disasters, with analysis results published annually on the website of the General Office of Building Control (2023). Between 1995 and 2023, a total of 9,807 building disasters were recorded. According to Article 73 of the Building Law (Dz.U. 2024 poz. 725), a building disaster is the unintended, sudden destruction of a construction object or its parts, including elements such as scaffolding, formwork, retaining walls, or excavation supports.

Reports on GINB (Główny Inspektor Nadzoru Budowlanego – Chief Inspector of Building Control) from 2019 to 2023 categorize the primary causes of such incidents into two groups. The first includes random events such as heavy rainfall, strong winds, landslides, or lightning strikes. The second involves human-related factors, including gas explosions, fires, and traffic accidents. Additionally, disasters can result from errors made during the operation or maintenance of buildings, as well as during the construction of new structures or renovations of existing ones. The most affected structural elements in disasters include walls, roofs, floor structures, and vertical load-bearing elements.

The Main Office of Building Control (GUNB) maintains a register of building disasters and publishes statistical reports; however, it does not disclose specific details such as the location, function, or history of the affected buildings. This information is often classified, with locations typically known only through media coverage.

Between 2019 and 2023, Poland recorded 1,889 building disasters, with twenty-three occurring in Warmia-Masuria (GINB, 2019, 2020, 2021, 2022, 2023). In Olsztyn, a part of this region, several incidents involved the collapse of buildings, primarily old tenement houses or structures undergoing renovation. The causes of these incidents were often related to poor technical conditions, improperly conducted construction work, a lack of adequate maintenance. The disasters occurred in various parts of the city, affecting ceilings, walls, or roof sections and, in some cases, requiring the evacuation of residents.

In this context, the European Ground Motion Service (EGMS), launched under the Copernicus program by the European Environment Agency (EEA), is a noteworthy tool (Larsen-NORCE et al., 2021). EGMS utilizes InSAR technology based on data from Sentinel-1 satellites to precisely monitor surface movements such as ground subsidence, terrain deformations, and tectonic shifts. The first version of this service was released in 2021, with the potential to become a widely used tool for analyzing ground movements across Europe. EGMS products are accessible via the EGMS Explorer platform (<https://egms.land.copernicus.eu/>) (Crosetto et al., 2023). This data can be used to assess the condition of buildings and infrastructure, identify areas with significant displacement, and plan modernization efforts (Kotzerke, 2022). Satellite analysis enables construction projects to be designed to minimize risks related to ground instability and optimizes designs by considering geological and geotechnical conditions. This translates into better durability, safety, and operational efficiency of structures.

Recent literature emphasizes the importance of InSAR technology, including EGMS, in infrastructure monitoring. Studies often integrate EGMS data with other methods, such as Permanent Scatterers InSAR (PSInSAR), and complement them with additional data types, such as LIDAR. Key research and advancements in infrastructure management focus on the integration of measurement data (He et al., 2021; Guoyang et al., 2024; Hlaváčová et al., 2023), applications in urban areas (Gao et al., 2022; Mele et al., 2023; Shahbazi et al., 2024a; Shahbazi et al., 2024b), monitoring buildings in mining and industrial regions (Nikolakopoulos et al., 2023), as well as progress in data processing and analysis (Festa et al., 2023; Hrysiewicz et al., 2024).

Despite the growing use of satellite data in research, practical systems that effectively integrate publicly available spatial data are still lacking. There is a need for simple and efficient tools that combine satellite data, geodetic measurements, and ground-based sensors to improve ground displacement monitoring, building assessment, and disaster

prevention. Although authorities conduct regular inspections, ground displacement analysis remains underused in risk management.

The research is grounded in the premise that modern technologies, particularly EGMS, can enhance urban safety by improving building monitoring and risk prevention. The study employed analytical methods to develop a displacement velocity and risk indicator model, utilizing satellite data (EGMS), LiDAR laser scanning, and GIS databases.

## Methods

The study aimed to identify buildings susceptible to deformations. The assessment model for determining buildings at risk of damage is designed to provide forecasts of potential infrastructure failures. In this context, satellite data from the European Ground Motion Service (EGMS) were used.

The proposed methodology consists of three stages:

### Stage 1: Development and Preparation of Satellite Data

The study utilized EGMS Level 2b (L2b) data from the five years 2019–2023. This calibrated product includes deformation velocities along the line of sight (LOS) and time series for ascending and descending geometries. Measurements were referenced to a deformation model derived from GNSS data, allowing for the calculation of absolute displacements. This stands in contrast to the L2a product, which does not incorporate corrections for tectonic activity or regional ground movements (Capes et al., 2023). The selection of L2b was justified by eliminating the influence of global or regional movements, increasing the precision of building displacement analysis.

Measurement Points (MPs) originate from both Sentinel-1 geometries: ascending (orbits 029 and 102) and descending (orbits 051 and 124). Based on the transformed equation (Wiczorek, 2019), the vertical component ( $MP_V$ ) and horizontal deformation ( $MP_H$ ) were calculated for each measurement point MP. The equations used for determining the actual components are presented below:

$$MP_V = \frac{\sin\theta^{desc} \cdot v_{los}^{asc} - \frac{\sin\theta^{asc}}{\cos\Delta\alpha} \cdot v_{los}^{desc}}{\cos\theta^{asc} \cdot \sin\theta^{desc} - \frac{\sin\theta^{asc} \cos\theta^{desc}}{\cos\Delta\alpha}} \quad (1)$$

$$MP_H = \frac{-\cos\theta^{desc} \cdot v_{los}^{asc} + \cos\theta^{asc} \cdot v_{los}^{desc}}{\cos\theta^{asc} \cdot \sin\theta^{desc} - \frac{\sin\theta^{asc} \cos\theta^{desc}}{\cos\Delta\alpha}} \quad (2)$$

Where  $V_{los}$  – deformation along LOS,  $MP_V$  – vertical deformation,  $MP_H$  – projection of horizontal deformation in descending azimuth look direction,  $\theta$  – incident angle,  $\Delta\alpha$  – satellite heading difference between ascending and descending mode.

The MP data were averaged within the building outline, following the EGMS L3 Ortho method (Ferretti et al., 2023). Building outlines were derived from LiDAR data and the Topographic Objects Database (BDOT10k – Baza Danych Obiektów Topograficznych).

EGMS technology aids in assessing building conditions and preventing structural failures, but has limitations, including limited geolocation accuracy and a sparse number of Measurement Points (MPs). Data quality depends on MP density, urban areas yield more precise results, while rural or mountainous regions are prone to greater errors due to atmospheric interference. Time series often contain noise, and geolocation precision is lower than deformation accuracy, which is critical for small structures. Single MP analyses are less reliable, making multi-point analysis essential for accurate risk assessment (Ferretti et al., 2023). In such cases, it is crucial to determine whether the MP corresponds to the location of the examined structure (Crosetto et al., 2023).

### **Stage 2: Building Extent and Height Determination**

LiDAR and BDOT10k data from 2023 were obtained from the Geoportal (<https://www.geoportal.gov.pl/>). The LiDAR dataset features a spatial density of 12 points/m<sup>2</sup>, with an average height error of 0.10 m, and an horizontal positioning error of 0.25 m. The data are referenced in the PL-1992 (horizontal) and PL-EVRF2007-NH (vertical) coordinate systems. The BDOT10k database, corresponding to a 1:10,000 scale map, provides information on building locations, number of floors, and intended use (Dz.U. 2021 poz. 1412). The vector file containing building polygons serves as a key input for further spatial analysis.

Actual building extents and heights were determined based on classified LiDAR points clouds. Since BDOT10k outlines do not account for protruding architectural elements (e.g., roof eaves, balconies, cantilevers, or ramps), LiDAR data were used to estimate the actual building boundaries. The reliability of this approach depends on the density of measurement points within each building footprint. To account for potential geolocation inaccuracies, an uncertainty buffer was applied based on the accuracy specifications of the EGMS data.

EGMS-S1 (Sentinel-1) features a pixel resolution of 14 m × 4 m (azimuth × range) and a standard height deviation ( $\sigma_{\text{localization}}$ ) of 2.1 m, reflecting the vertical localization uncertainty of, for Example, a PS point in SAR data. 5 m buffer was established based on the 2.1 m deviation ( $2.1 \text{ m} \times 2.38 \approx 5 \text{ m}$ ), corresponding to 2-3 times the standard deviation ( $2\sigma$ - $3\sigma$  rule), covering 95-99% of cases with a safety margin (Costantini et al., 2014). The

buffer defines the area around a building where MP points are considered representative, minimizing localization errors, such as ground points being mistaken for rooftop points. Due to the lower more significant height deviation in EGMS, a 5 m buffer is required for the effective selection of MP points.

The height of each MP's building was estimated based on the height difference model between the EGM2008 and PL-EVRF2007-NH vertical reference systems obtained from the QGIS repository (Convert Heights tool developed in 2021 by Warsaw University of Technology).

Building heights from LiDAR were validated using a  $\pm 0.5$  m buffer, in line including (Dz.U. 2023, item 89) and ASPRS (American Society for Photogrammetry and Remote Sensing) standards, which recommend 95% confidence for classification accuracy ( $\pm 0.15$ – $0.30$  m). MP elevations were compared to LiDAR heights, and outliers were excluded. Verified MP points were then clipped to updated building boundaries, retaining only those belonging to actual structures.

### Stage 3: Calculation of the Building Risk Index (BRI)

The risk for a building can be defined as a function of displacement velocity ( $MP_v$ ,  $MP_H$ ), measurement point density ( $\rho_{MP}$ ), *slope* and *aspect* (formula 4):

$$BRI = w_1 \cdot |MP_V| + w_2 \cdot |MP_H| + w_3 \cdot \frac{1}{\rho_{MP}} + w_4 \cdot slope + w_5 \cdot aspect \quad (3)$$

Where:  $|MP_v|$ ;  $|MP_H|$  – absolute deformation velocity values in respective directions (mm/year);  $\rho_{MP}$  – inverse measurement points density (pkt/m<sup>2</sup>); *slope* – terrain slope angle in degrees (0–90°); *aspect* – slope orientation in degrees (0–360°), relative to north;  $w_1$ ,  $w_2$ ,  $w_3$ ,  $w_4$ ,  $w_5$  – empirically determined weights.

A lower number of MPs increases uncertainty and raises the risk. An important factor is the number of MP measurement points per unit area of the building. Point density is a reliability measure of data; the higher the density, the greater the confidence in estimating deformations, reducing the risk of errors. The adopted model includes all buildings, even those with a single point, as the risk index incorporates a weight.

As part of the terrain topography analysis in the risk model, slope and aspect parameters were calculated based on LiDAR data and the digital terrain model (DTM) to account for them in the risk assessment of deformations. These parameters influence the ground and building stability in Olsztyn, where natural conditions such as lakes, forests, and rivers play a significant role. Steeper terrain increases the risk of landslides and deformations, especially during heavy rainfall, while slope exposure affects wind and solar energy.

The slope in degrees (0–90°) was calculated based on the height gradient between neighboring points from LiDAR data and then normalized to a 0–1 scale (slope/90), where 0 represents flat terrain, and 1 represents a vertical slope.

The slope direction in degrees (0–360°) was transformed into a risk measure on a 0–1 scale. The dominant westerly and southwesterly winds (225°–315°) (Dygulska et al., 2015; IMGW accessed 2024) increase erosion risk and load on slopes facing these directions. Hence, they were assigned a value of 1.0. Stable northern directions (0°–45° and 315°–360°), sheltered from the wind, received a value of 0.5, while other directions (east, south, 45°–225°) with moderate risk were assigned 0.75.

Empirical weights were applied due to the early stage of the research and the limited amount of available data in Olsztyn, only 10 incidents were recorded between 2019 and 2023, most of which were temporary (e.g., roof or ceiling repairs), not indicative of lasting risk, as illustrated in Case II of the article. The data primarily came from media sources, since official reports do not disclose full information about the locations. The weights ( $w_1 = 0.35$ ,  $w_2 = 0.30$ ,  $w_3 = 0.10$ ,  $w_4 = 0.15$ ,  $w_5 = 0.10$ ) were determined through an iterative process, achieving 80–90% consistency with test data, which enabled effective classification of buildings (9 high-risk, 56 medium-risk). The empirical approach was simple and tailored to Olsztyn's local conditions; however, in the future, with a larger dataset, the use of statistical methods such as regression is planned to enhance objectivity.

The risk was categorized into three levels: low (<2), medium (2–4), and high (>4). The model was visualized in a GIS system as a risk map, where buildings were marked with low, medium, and high risk values. The model validation was conducted by comparing its results with actual incidents in Olsztyn from 2019 to 2023. The outcome is a risk map and a list of at-risk buildings.

For risk assessment and identification of endangered buildings, a parameter defining the deformation rate displacement velocity was used to assess risk and identify endangered buildings. Deformation velocity was selected as the primary measure due to its stability and precision in determining changes (Shahbazi et al., 2024b). The deformation measurement over time  $D(x, y, t)$  was performed based on a time series for individual MPs, focusing exclusively on buildings with high-risk indexes (formula 4).

$$D(x, y, t) = \int_{t_0}^t V_{los}(x, y, \tau) d\tau + D_0(x, y) \quad (4)$$

Where:  $D(x, y, t)$  – total displacement at a point with coordinates  $(x, y)$  at time  $t$  (w mm);  $V_{LOS}(x, y, \tau)$  – displacement velocity in the line of sight (LOS) from EGMS, variable over time  $\tau$ , calibrated against GNSS data (mm/yr);  $t_0$  – initial time point (year 2019);  $t$  – current time point;  $D_0(x, y)$  – initial deformation, calibrated against GNSS.

## Results

The procedure results were presented based on a specific case study in Olsztyn, a city in Warmia-Masuria in northeastern Poland. The city's spatial structure derives from historically shaped settlement systems, including the medieval old town with its suburbs and elements associated with its later development, such as railway infrastructure, barracks, residential estates, and former villages gradually incorporated into Olsztyn's administrative boundaries. The contemporary character of the city's development is primarily determined by natural conditions, such as numerous lakes, extensive forests, and rivers, which limit opportunities for intensive urbanization, favoring smaller-scale investments (development strategy). The central part of the city primarily serves residential and service functions, dominated by historic tenement houses and low-rise buildings. Industrial and service facilities prevail in the northeastern part, while extensive residential districts with high-rise multifamily buildings characterize the southern part. The western zone of Olsztyn, adjacent to former village areas, stands out with lower-density housing estates, where single-family homes predominate. A map of Olsztyn is shown in Figure 2.

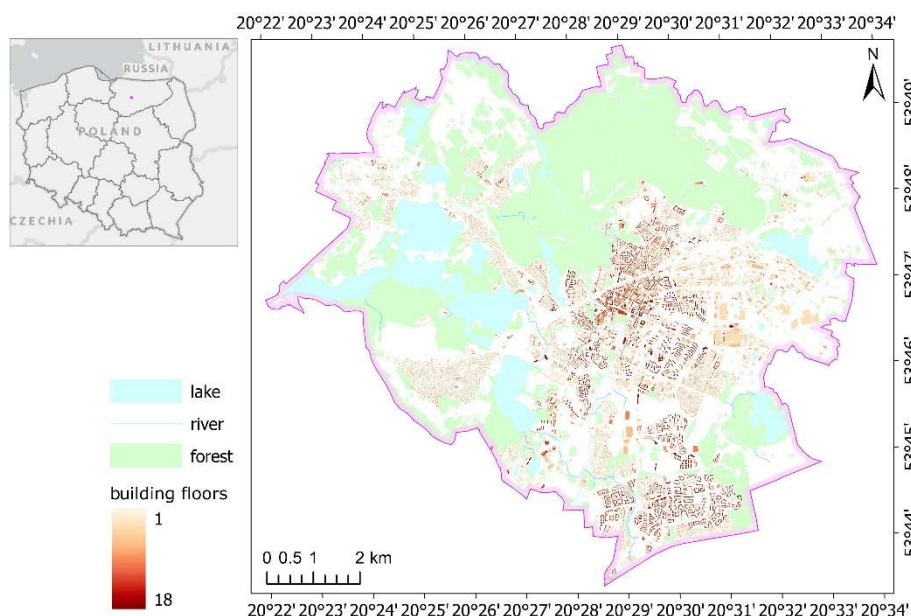


**Fig. 1.** Location of the study area in Olsztyn with information on buildings' heights.

The distribution of building categories in Olsztyn is as follows: 98.04% are operational buildings, 0.09% are destroyed objects, 0.92% are inactive buildings, and 0.95% are under construction.

After analyzing and verifying the association of MP points with building areas, the visualization of outlier points is shown in Figure 2. For the ascending geometry, 70% of the points were retained, while for the descending geometry, 71% of the points were retained. The figure shows that areas adjacent to lakes and forests are dominated by negative height differences between buildings and MP points, indicating that these points are located above the buildings (marked in red).

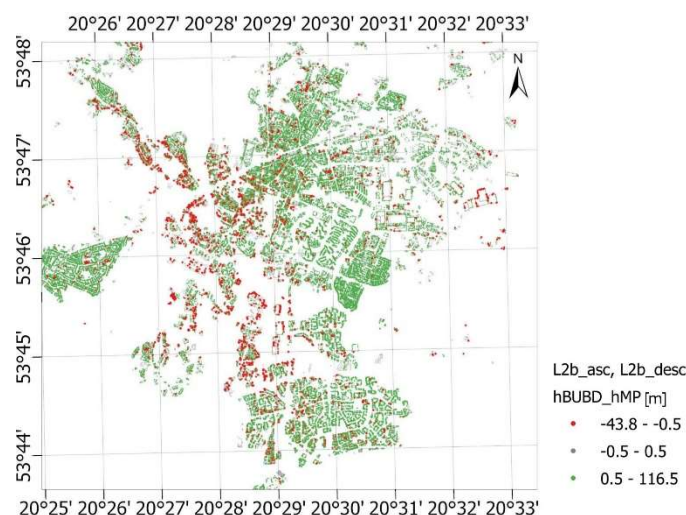
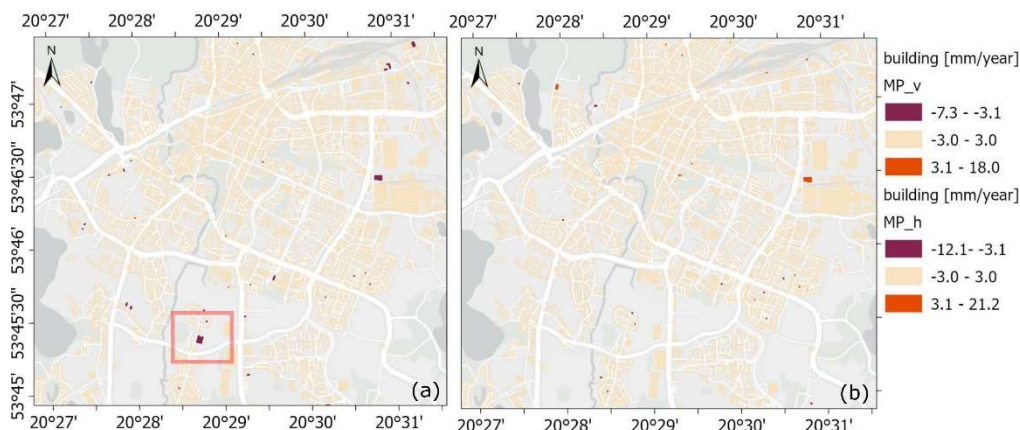


**Fig. 2.** Visualization of the spatial distribution of outlier points above and below the building that fall outside the buffer criterion.

Some buildings were omitted from the analysis due to a lack of measurement points (MP). Displacement velocities were determined for 86.31% of the buildings, with values in the Olsztyn area ranging from  $-7$  mm/year to  $+18$  mm/year for the vertical component and from  $-12$  mm/year to  $+21$  mm/year for the horizontal component between 2019 and 2023. The standard deviation for the data in both geometries was established at  $\pm 0.63$  mm/year and  $\pm 0.66$  mm/year, respectively. It was assumed that displacements within the  $\pm 3$  mm/year range would not be subject to further studies, as they fall within the typical deformation range in Poland, according to Naumowicz et al. (2024).

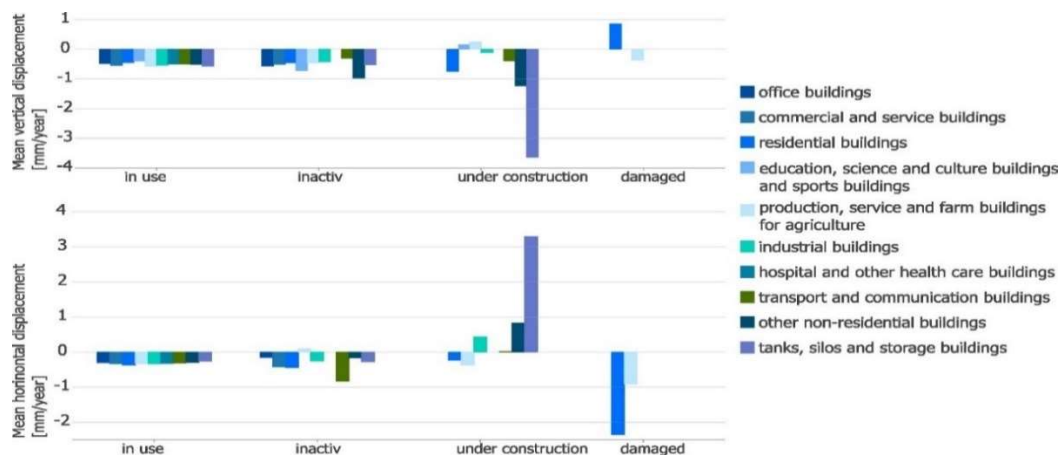
The buildings in the analyzed area that exhibit significant displacement velocities are not evenly distributed and do not follow any characteristic spatial pattern. Such a distribution may result from the influence of various factors, such as local geological conditions, anthropogenic loads (e.g., intensive land use), or differences in the construction and age of the buildings. Figure 3 shows a section of the map illustrating objects with high displacement velocity values in both directions.

(b)



**Fig. 3.** The displacement velocity maps for individual buildings with significantly deviating velocity values after excluding velocities within the  $\pm 3$  mm/year range. (a) the actual displacement vector velocity for the vertical component and (b) for the horizontal component.

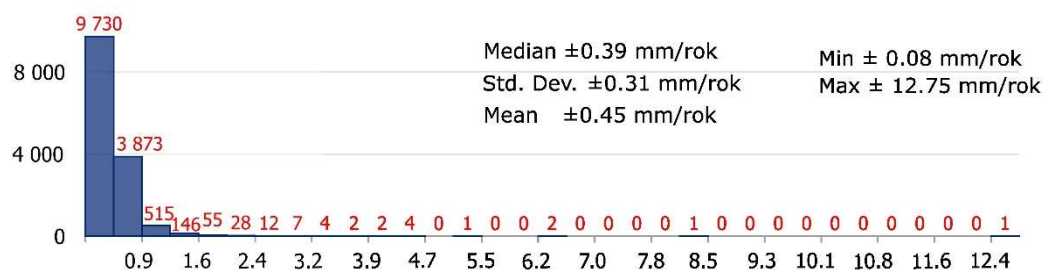
Construction structures with elevated displacement velocity values are located on the outskirts of Olsztyn, in districts with a service and industrial character, which may suggest the presence of industrial facilities. Due to its large footprint, the building marked with a red outline in Figure 3a could be considered an industrial facility. However, it is a residential building with a closed layout and additional internal courtyards. Across the city, varying changes in the technical condition of buildings can be observed. The analysis of these changes is presented in Figure 4, where the graphs show the average vertical and horizontal displacements for different types of buildings, taking their status into account.



**Fig. 4.** Mean displacement speed categorized by building existence and function.

Damaged buildings exhibit the greatest vertical and horizontal displacements, indicating their significant susceptibility to structural instability resulting from material degradation, previous damage, or the impact of unfavorable environmental conditions. In contrast, operated and inactive buildings remain more stable, which may be linked to regular maintenance in the case of operated structures or the absence of ongoing loads in inactive ones. These observations confirm the usefulness of data obtained from EGMS technology.

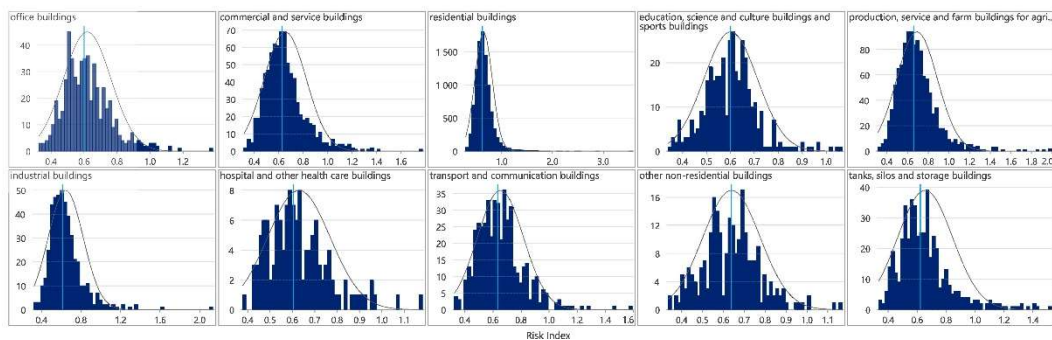
A zonal analysis was conducted for the buildings, determining slope and exposure parameters, which were included in the risk model. Each building was assigned to the appropriate categories. A map showing buildings with an assigned Building Risk Index (BRI) was prepared on a scale from 1 to 3. Of 14,383 analyzed buildings, only 9 were classified as high risk and 56 as medium risk. Statistical results of the risk index are presented in Figure 5.



**Fig. 5.** Building Risk Index (BRI) graph with the number of objects at different risk levels.

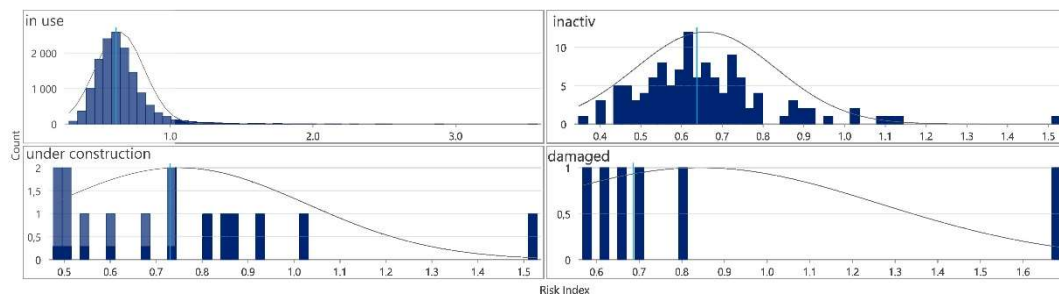
The vast majority of buildings show very low risk index values. The largest group of buildings (9,730) falls within the 0.1–0.5 range, indicating a low risk of changes for most structures. The low median and average values suggest that the overall risk is generally low for most buildings, though a few cases require detailed analysis.

Figure 6 shows the risk index distribution for different building types, considering their functional use. In most categories, the risk index distribution resembles a normal distribution with slight asymmetry. Buildings with low-risk indices prevail, suggesting that threats from natural or structural factors are not common. In some categories, outliers on the right side indicate a few objects with increased risk. The highest number of such buildings is noted among residential and industrial objects.



**Fig. 6.** Distribution of risk by building function (the horizontal axis represents the risk index, while the vertical axis indicates the number of buildings).

The relationship between the BRI index and different building existence categories was analyzed (Figure 7). The most numerous category consists of operational buildings, for which the risk index is relatively low. Inactive buildings show more significant risk dispersion, likely due to their technical condition. Buildings under construction and damaged buildings have irregular risk index distributions due to the small number of objects in these groups (21 objects). Outliers in each category indicate buildings with significantly increased risk that may require additional analysis.



**Fig. 7.** Risk indicator of settlement or damage to buildings, depending on their operational condition.

#### Justification for Case Selection:

Case I presents a building marked in Figure 3(a) experiencing systematic settlement ( $-14.46$  mm/ $-17.62$  mm over 4.88 years), which confirms the effectiveness of the BRI model in identifying risks associated with persistent deformations, even when the structure is classified as medium risk.

Case II involves a building that suffered a structural failure in 2019; its low BRI index (0.36) and lack of a clear deformation trend ( $-3.08$  mm over 5.87 years) indicate an incidental nature of the event. This highlights the importance of distinguishing between ongoing and temporary risks.

The comparison of these contrasting cases emphasizes the difference between structures requiring continuous monitoring and those no longer posing a threat, thereby reinforcing the credibility of the BRI approach.

**Case I:** The analysis includes a building classified as a medium-risk object (Figure 3(a)). Its actual displacement speed is approximately  $\pm 3.23$  mm/year. Time series were developed for this complex and averaged for each geometry – ascending (207 points) and descending (111 points) – based on data from four orbits (29A, 102A, 51D, 124D) covering the period from 2019 to 2023. The analysis results are presented in Figure 8.

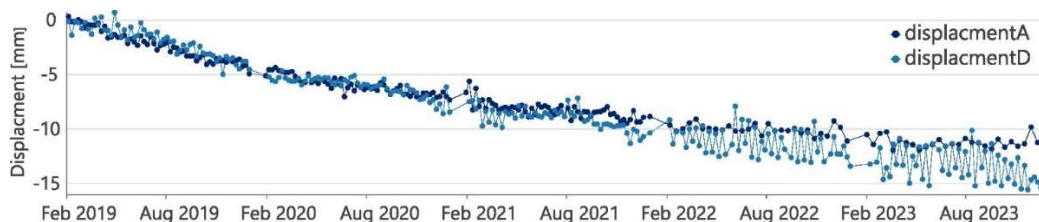


**Fig. 8.** Building displacement velocity in the line of sight (LOS), determined based on averaged values for ascending and descending geometries.

The calculated mean velocity for the cumulative deformation velocity is  $-2.30$  mm/year with a standard deviation of  $\pm 0.17$  mm/year for the ascending geometry and  $-2.89$  mm/year with a standard deviation of  $\pm 0.20$  mm/year for the descending geometry. This building complex was constructed in 2019; it has three above-ground stories and one underground level. It can be said that this building has been systematically settling since its inception. From March to April 2020, a sudden settlement occurred, with deformation changes exceeding  $-6$  mm, with measurements taken every six days. Since June 2021, the settlement has exceeded  $-10$  mm; since then, the building has maintained a constant settlement velocity.

The analysis involves calculating the time series deformation based on the deformation formula from Equation 4. The initial value  $D_0$  was assumed to be 0.

Observation period assumption: The time vector (years) for the ascending geometry has 209 values for this building, meaning the velocity vector ( $v_{los}$ ) contains 209 displacement values (in mm), representing the average velocities for each time interval. For the second geometry, the number of time points is 156. The deformation ( $D$ ) is  $-11.23$  mm and  $-14.28$  mm, respectively. The negative value indicates ground subsidence along the line of sight (LOS) from February 2019 to December 2023.

Based on separate calculations (the vertical component ( $D_{wp}$ )) for each geometry, it was found that the building subsided vertically by approximately 14.46 mm (ascending) and 17.62 mm (descending) over 4.88 years. The differences in deformation magnitude result

from the different number of observations for the study period (209 and 156) and the varying number of points for which the series were averaged (207 and 111).

Comparing the *mean\_velocity* of  $-2.30$  mm/year and  $-2.89$  mm/year with  $\Delta t \approx 4.88$  years and calculating linear deformation yields results of approximately  $-11.24$  mm and  $-14.11$  mm. The integration results ( $-11.23$  mm and  $-14.28$  mm) are very close to the linear values ( $-11.24$  mm and  $-14.11$  mm), suggesting that the deformation is linear with minimal deviations (e.g., seasonal). This building underwent deformation of  $-11.23$  mm ( $-14.28$  mm) from February 2019 to December 2023. The vertical subsidence of the building is  $14.46$  mm ( $17.62$  mm).

Verification was conducted by calculating the RMSE, which determines the level of uncertainty. For the first dataset, the RMSE value is  $\pm 3.09$  mm, giving a deformation range of  $-8.14$  mm to  $-14.32$  mm, while for the second dataset, the RMSE is  $\pm 3.49$  mm, covering a range from  $-10.79$  mm to  $-17.77$  mm.

**Case II:** In February 2019, construction work led to a disaster threatening the collapse of a four-story residential building constructed in 1988.

This study analyzed 2019–2023, with early 2019 as the reference point for assessing the building's current technical condition after this disaster. Additional EGMS data from 2018–2022 was included, allowing the analysis of the building's earlier condition. Examining this extended period enabled the assessment of displacement trends in the structure. For this purpose, time series from the two periods were combined into a single dataset. Approximately five measurement points from different geometries were selected for each dataset. However, data for geometry 124D from 2018–2022 was unavailable. A total of 33 measurement points were used for the analysis.

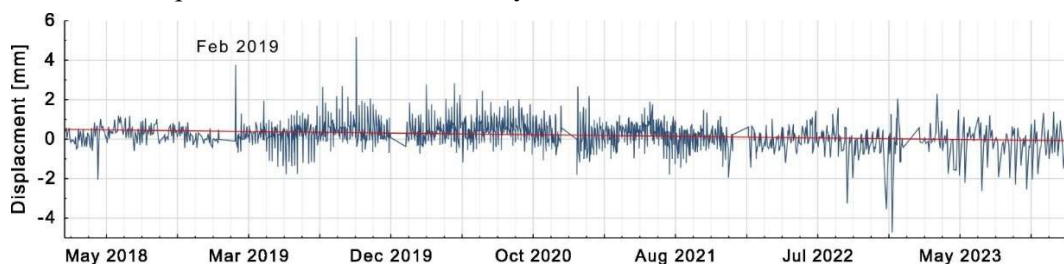


**Fig. 9.** The chart presents a detailed record of displacement measurements obtained from multiple measurement points (MP) in various satellite geometries, including both ascending and descending orbits of the Sentinel-1 satellites. This data, collected from February 2018 to December 2023, illustrates the trends in the building's displacements.

In the time series graph of the building's deformation, an incident from February 2019 is visible, as well as individual jumps and anomalies, such as sudden deviations above  $+4$

mm or below -4 mm. Periods of greater anomalies should be analyzed to investigate their causes. The overall trend suggests stability of displacements over the long term. The red line indicates that the average displacement remains close to zero throughout the period, which confirms the lack of a clear trend. Minor local changes are possible; however, no distinct direction of changes (either increase or decrease) is observed. In the risk model, this building received an index of 0.36.

The total deformation of the building from February 6, 2018, to December 19, 2023, is -3.08 mm, indicating that the object has lowered in the line of sight (LOS) by 3.075 mm over approximately 5.87 years.

Based on an average deformation rate of -0.21 mm/year (with a standard deviation of  $\pm 0.19$  mm/year), the expected value of deformation for this period is approximately -1.26 mm. The difference between the value resulting from the integration of the deformation rate (-3.08 mm) and that calculated based on the average rate (-1.26 mm) suggests the presence of fluctuations, such as seasonality that are not accounted for in a simple average rate model.

The calculated RMSE value of the trend is 3.68 mm, indicating some data dispersion; however, this does not affect the final value of deformation. The confidence interval for the total deformation ranges from -6.75 mm to +0.60 mm.

The building did not receive a high risk index, suggesting little movement. This may indicate that while there are some deviations over time, they do not point to a significant threat to its structural stability.

## Discussion

The study focused on the key significance of the European Ground Motion Service (EGMS) technology in assessing the technical condition of buildings and preventing potential construction disasters. EGMS, as an advanced tool based on Interferometric Synthetic Aperture Radar (InSAR) data, provides precise information on large-scale ground deformations, enabling monitoring of Earth surface movements with millimeter-level accuracy. Regular evaluation of the technical state of buildings using EGMS allows for the early detection of damage, which is crucial for preventing serious structural problems that could lead to disasters.

This paper proposes a risk assessment model based on EGMS satellite data that can be used to identify buildings at risk of damage due to structural instability or changes in their surroundings.

As part of the study, a risk model was developed to determine risk indicators for different types of buildings, considering their function (e.g., residential, industrial, public utility) and the state of their existence, such as operational, under construction, inactive, or destroyed.

A key element of the model was the actual displacement rate, determined based on the line-of-sight (LOS) velocity components from ascending and descending tracks. This rate was calculated as a vector of actual surface movement, enabling the reconstruction of multidimensional displacements based on one-dimensional LOS data. This method, described in the literature (Crosetto et al., 2020), allows for more precise geophysical analyses, considering vertical movements (e.g., subsidence or uplift) and horizontal shifts.

The model was tested on buildings in Olsztyn, where risk indicators on a scale from 1 to 3 (low, medium, high) were calculated based on EGMS data. The model's usefulness in identifying potential threats was demonstrated in two analyzed cases (Case I and Case II). In Case I (Figure 8), discrepancies in displacement values depending on track geometry (ascending and descending) were noted, which may be related to terrain slope direction. The range of determined deformation varies significantly: from  $-8.14$  mm to  $-14.32$  mm for the ascending track and from  $-10.79$  mm to  $-17.77$  mm for the descending track. In Case II, the building received a low-risk index, suggesting that its displacements remain within an acceptable range. According to construction standards (Eurocode 7), permissible vertical displacements (subsidence) typically range from 10–20 mm throughout the building's operational period, depending on the type of construction and intended use of the facility. Although some deviations occurred over time, they do not indicate significant deterioration of the building's technical condition. However, in more prominent anomalies, it would be necessary to analyze causes such as measurement errors, environmental changes (e.g., temperature, loads), or random events (e.g., seismic movements).

The proposed model can be enhanced by incorporating additional features to improve its accuracy and applicability. Several important directions for refining data integration and analysis are outlined below:

1. Use of Total Deformation  $D(x,y,t)$ : Unlike mean deformation velocity, total deformation, expressed in millimeters, captures the full displacement over the observation period, including seasonal changes. This cumulative metric offers a more realistic view of ground movement, which is vital for assessing building damage risks. In Case II,  $D(x,y,t)$  more effectively reflected the building's structural impact, while velocity trends aided long-term forecasting.

2. Track Geometry Consideration: InSAR data utility varies by track orientation and terrain slope. Ascending tracks favor west-facing slopes; descending tracks suit east-facing ones (Ferretti et al., 2007). Combining both improves data interpretation. The model should evaluate each geometry's relevance based on local terrain and apply appropriate weighting.

In Case I (Figure 8), deformation differences stemmed from radar foreshortening (Ferretti et al., 2023).

3. **Deformation Gradient Analysis:** Calculated from mean velocities, the deformation gradient highlights local displacement differences that may stress structures (Shahbazi et al., 2024a; 2024b). This parameter is crucial for identifying risk in vulnerable zones, such as those affected by faults or mining. Including it enables finer-grained building condition assessments.

4. **Integrating Building Technical Condition Data:** Although the study highlights the importance of EGMS in monitoring and preventing building failures, the current model lacks data on technical building conditions. Factors such as building age, structural integrity, material types, renovation history, and other parameters (e.g., year of construction, height, number of floors, building use) are essential for accurate risk evaluation.

5. **Incorporating Environmental and Geological Data:** Environmental factors, such as temperature variations, precipitation, soil moisture, and wind loads, can significantly impact structural stability and should be included in the analysis. Geological data, including soil type (e.g., clay, sand, rock), presence of tectonic faults, groundwater levels, and seismic activity, are also critical in identifying causes of displacement and their effects on buildings.

To adapt the model to local conditions, parameter weights can be determined using statistical methods, such as linear/logistic regression (for disaster prediction) or correlation analysis (to assess parameter dependencies). The statistical approach is precise but requires large data volumes – in Olsztyn, 10 construction incidents were recorded between 2019 and 2023 (vs. 1889 in Poland, GUNB), which limits its application. The current model is based on an empirical approach, but it is planned to expand with statistical methods using GUNB data. To enhance the credibility of the BRI method, it is essential to account for the difference between structures undergoing long-term settlement (requiring continuous monitoring) and those that have experienced past but currently irrelevant risks.

In conclusion, integrating these diverse data sources will create a more comprehensive risk model that better reflects actual building threats in various environmental and geological conditions.

## Conclusions

The European Ground Motion Service (EGMS) provides an effective technological solution for assessing building conditions and preventing construction disasters. By supplementing traditional displacement and deformation measurements with continuous,

wide-area satellite monitoring, EGMS significantly enhances the efficiency and precision of large-scale structural assessments.

A risk model utilizing EGMS data enables the identification of buildings most vulnerable to structural damage. A case study in Olsztyn demonstrated EGMS's ability to improve risk assessment accuracy through early anomaly detection, facilitating timely preventive measures to ensure structural safety and integrity.

Integration of EGMS with databases like the GUNB construction disaster register (2023) supports the development of robust risk models. However, broader implementation requires improved data accessibility and user-friendly platforms. A current limitation is the geolocation accuracy of measurement points, which may affect reliability, particularly for smaller structures.

When combined with AI, BIM, and IoT technologies, EGMS forms part of an advanced, comprehensive infrastructure monitoring system, substantially improving both safety standards and management capabilities.

## References

- Capes, R., Passera, E., 2023. Product Description and Format Specification. *End-to-end implementation and operation of the European Ground Motion Service (EGMS)*
- Costantini, M., Falco, S., Malvarosa, F., Minati, F., Trillo, F., Vecchioli, F. 2014. Persistent Scatterer Pair Interferometry: Approach and Application to COSMO-SkyMed SAR Data, in *IEEE Journal of Selected Topics in Applied Earth Observations and Remote Sensing*, vol. 7, no. 7, 2869-2879. <https://doi.org/10.1109/JSTARS.2014.2343915>.
- Crosetto, M., Solari, L. 2023. Satellite Interferometry Data Interpretation and Exploitation Case Studies From The European Ground Motion Service (EGMS). *BOOK Elsevier*. <https://doi.org/10.1016/c2022-0-01853-5>
- Crosetto, M.; Solari, L.; Mróz, M. 2023. Pan-European Deformation Monitoring: The European Ground Motion Service. *En 5th Joint International Symposium on Deformation Monitoring (JISDM 2022)*. Editorial Universitat Politècnica de València. 383-388. <https://doi.org/10.4995/JISDM2022.2022.13876>
- Dygulska, A., Perlańska, E. 2015. Ochrona Środowiska III. Mapa wietrzności Polski Projekt Czysta Energia Akademickie Centrum Czystej Energii. Dygulska, A., Perlańska, E. 2015. Environmental Protection III. Windiness Map of Poland, Clean Energy Project, Academic Clean Energy Center.
- Dz. U. 1994 Nr 89 poz. 414. Ustawa z dnia 7 lipca 1994 r. Prawo budowlane. *Dz.U. 2024 poz. 725*. Journal of Laws 1994 No. 89, item 414. Act of July 7, 1994, Construction Law. Journal of Laws 2024, item 725.
- Dz.U. 2021 poz. 1412. Rozporządzenie Ministra Rozwoju, Pracy i Technologii z dnia 27 lipca 2021 r. w sprawie bazy danych obiektów topograficznych oraz bazy danych obiektów

- ogólnogeograficznych, a także standardowych opracowań kartograficznych. *Journal of Laws* 2021, item 1412. Regulation of the Minister of Development, Labor and Technology of July 27, 2021, regarding the database of topographic objects and the database of general geographic objects, as well as standard cartographic studies.
- Dz.U. 2023 poz. 89 . Rozporządzenie Ministra Rozwoju i Technologii z dnia 16 grudnia 2022 r. w sprawie baz danych dotyczących zobrazowań lotniczych i satelitarnych oraz ortofotomapy i numerycznego modelu terenu. *Journal of Laws* 2023, item 89. Regulation of the Minister of Development and Technology of December 16, 2022, regarding databases concerning aerial and satellite imagery, as well as orthophotomaps and digital terrain models.
- EGMS Explorer. Available online: (<https://egms.land.copernicus.eu/>) (accessed on 18.10.2024)
- Eurokod 7 (PN-EN 1997-1:2008) (Geotechnika – nośność i osiadanie) (Geotechnics – bearing capacity and settlement)
- Ferretti, A., Monti-Guarnieri, A., Prati, C., Rocca, F. 2007. InSAR Principles: Guidelines for SAR Interferometry Processing and Interpretation. *European Space Agency*
- Ferretti, A., Passera, E., Capes, R. 2023. Algorithm Theoretical Basis Document. *End-to-end implementation and operation of the European Ground Motion Service (EGMS)*
- Festa, D., & Del Soldato, M. (2023). EGMStream, a Desktop App for EGMS Data Downstream. *Remote Sensing*, 15(10), 2581. <https://doi.org/10.3390/rs15102581>
- Gao, Q.; Crosetto, M.; Monserrat, O.; Palama, R.; Barra, A. 2022. Infrastructure Monitoring Using the Interferometric Synthetic Aperture Radar (INSAR) Technique. *The International Archives of the Photogrammetry, Remote Sensing and Spatial Information Sciences*. 43, 271–276. <https://doi.org/10.5194/isprs-archives-XLIII-B3-2022-271-2022>
- Geoportal. Available online: (<https://www.geoportal.gov.pl/>) (accessed on 17.10.2024)
- Główny Inspektor Nadzoru Budowlanego (GINB). 2023. Katastrofy budowlane w 2023 roku. *Główny Urząd Nadzoru Budowlanego (GUNB)*. Chief Inspector of Building Control (GINB). Construction Disasters in 2023. *Main Office of Building Control (GUNB)*.
- Główny Inspektor Nadzoru Budowlanego (GINB). 2022. Katastrofy budowlane w 2022 roku. *Główny Urząd Nadzoru Budowlanego (GUNB)*. Chief Inspector of Building Control (GINB). Construction Disasters in 2022. *Main Office of Building Control (GUNB)*.
- Główny Inspektor Nadzoru Budowlanego (GINB). 2021. Katastrofy budowlane w 2021 roku. *Główny Urząd Nadzoru Budowlanego (GUNB)*. Chief Inspector of Building Control (GINB). Construction Disasters in 2021. *Main Office of Building Control (GUNB)*.
- Główny Inspektor Nadzoru Budowlanego (GINB). 2020. Katastrofy budowlane w 2020 roku. *Główny Urząd Nadzoru Budowlanego (GUNB)*. Chief Inspector of Building Control (GINB). Construction Disasters in 2020. *Main Office of Building Control (GUNB)*.
- Główny Inspektor Nadzoru Budowlanego (GINB). 2019. Katastrofy budowlane w 2019 roku. *Główny Urząd Nadzoru Budowlanego (GUNB)*. Chief Inspector of Building Control (GINB). Construction Disasters in 2019. *Main Office of Building Control (GUNB)*.
- Guoyang W., Peng L., Zhenhong L., Jie L., Yi Z., Houjie W. 2024, InSAR and machine learning reveal new understanding of coastal subsidence risk in the Yellow River Delta. China, *Science of The Total Environment*, 915. <https://doi.org/10.1016/j.scitotenv.2024.170203>

- He, Y., Xu, G., Kaufmann, H., Wang, J., Ma, H., & Liu, T. 2021. Integration of InSAR and LiDAR Technologies for a Detailed Urban Subsidence and Hazard Assessment in Shenzhen, China. *Remote Sensing*, 13(12), 2366. <https://doi.org/10.3390/rs13122366>
- Hlaváčová, I., Kolomazník, J., Struhár J., Orlitová, E. 2023. InSAR Ground Motion Mapping in Support of Urban Resilience and Regional Landscape Planning. *Joint Urban Remote Sensing Event (JURSE)*, 1-4. <https://doi.org/10.1109/JURSE57346.2023.10144209>
- Hrysiewicz, A., Khoshlahjeh Azar, M., Holohan, E.P. 2024. EGMS-toolkit: a set of Python scripts for improved access to datasets from the European Ground Motion Service. *Earth Science Informatics* 17, 3825–3837. <https://doi.org/10.1007/s12145-024-01356-w>
- IMGW (Instytut Meteorologii i Gospodarki Wodnej Państwowy Instytut Badawczy). Available online: <https://imgw.pl/edukacja/slowniki-hydrologiczno-meteorologiczne/> (accessed on 10.10.2024). Institute of Meteorology and Water Management, National Research Institute (IMGW)
- Kotzerke, P., Siegmund, R., Langenwalter, J. 2022. Product User Manual. *End-to-end implementation and operation of the European Ground Motion Service (EGMS)*
- Larsen-NORCE, Y., Bishop, C., Jøkulsson, G., Gjøvik Kongsberg, L.-P., Frauenfelder, R., Salazar, S. E. 2021. Geotechnical, LAND MONITORING SERVICE, *European Ground Motion Service: Service Implementation Plan and Product Specification Document*
- Mele, A., Crosetto, M., Miano, A., & Prota, A. (2023). ADAfinder Tool Applied to EGMS Data for the Structural Health Monitoring of Urban Settlements. *Remote Sensing*, 15(2), 324. <https://doi.org/10.3390/rs15020324>
- Naumowicz., B., Kowalczyk, K., Pelc-Mieczkowska. R. 2024. PPP solution-based model of absolute vertical movements of the Earth's crust in Poland with consideration of geological, tectonic, hydrological and mineral information. *ESS Open Archive*. <https://doi.org/10.22541/essoar.173046842.26349555/v1>
- Nikolakopoulos, K. G., Kyriou, A., Koukouvelas, I. K., Tomaras, N., Lyros, E. 2023. UAV, GNSS, and InSAR Data Analyses for Landslide Monitoring in a Mountainous Village in Western Greece. *Remote Sensing*, 15(11), 2870. <https://doi.org/10.3390/rs15112870>
- Shahbazi, S., Barra, A.; Gao, Qi.; Crosetto, M. 2024a. Detection of buildings with potential damage using differential deformation maps, Volume 218, Part B, 57-69. *ISPRS Journal of Photogrammetry and Remote Sensing*. <https://doi.org/10.1016/j.isprsjprs.2024.10.008>
- Shahbazi, S., Barra, A., Navarro, J. A., Crosetto, M. 2024b. From EGMS Data to a Differential Deformation Map For Buildings at Continent Level. *Procedia Computer Science*, 239, 2150-2157. <https://doi.org/10.1016/j.procs.2024.06.403>
- Uchwała Nr LI/816/22 Rady Miasta Olsztyna z dnia 28 września 2022 r. Załącznik: Strategia Rozwoju Miasta – Olsztyn 2030+. Uchwała Nr LI/816/22 Rady Miasta Olsztyna z dnia 28 września 2022 r. Załącznik: Strategia Rozwoju Miasta – Olsztyn 2030+.
- Wieczorek, B. (2020). Evaluation of deformations in the urban area of Olsztyn using Sentinel-1 SAR interferometry. *Acta Geodynamica et Geomaterialia* 17, 5–18. <https://doi.org/10.13168/AGG.2019.0041>

### **Streszczenie**

*W niniejszym badaniu przeanalizowano wykorzystanie technologii European Ground Motion Service (EGMS) do oceny stanu technicznego budynków oraz zapobiegania katastrofom konstrukcyjnym, ze szczególnym uwzględnieniem Olsztyna w Polsce w latach 2019–2023. Na podstawie danych satelitarnych EGMS opracowano model oceny ryzyka, umożliwiający identyfikację budynków podatnych na uszkodzenia wynikające z niestabilności konstrukcyjnej spowodowanej czynnikami antropogenicznymi lub naturalnymi, przy czym konkretne przyczyny nie zostały przeanalizowane. Analiza przeprowadzona w Olsztynie, obejmująca 14 383 budynki, ujawniła istotne zmiany przemieszczeń. Największe wartości odnotowano w budynkach uszkodzonych, gdzie prędkości ruchu wynosiły od  $-7,3$  mm/rok do  $+18$  mm/rok dla składowej pionowej oraz od  $-12,3$  mm/rok do  $+21,2$  mm/rok dla składowej poziomej. Tak wysokie wartości wskazują na znaczący wpływ czynników takich jak niestabilne podłoże, uszkodzenia konstrukcyjne czy oddziaływanie środowiskowe (np. osuwiska, wibracje), co zwiększa ryzyko dalszej degradacji tych obiektów. Z kolei budynki użytkowane (98,04%) oraz nieaktywne (0,92%) wykazują większą stabilność, a ich przemieszczenia zazwyczaj nie przekraczają  $\pm 3$  mm/rok. Wśród analizowanych obiektów dziewięć sklasyfikowano jako budynki wysokiego ryzyka, a 56 jako budynki średniego ryzyka. Walidacja przeprowadzona na podstawie historycznych zapisów dotyczących katastrof budowlanych w Olsztynie w badanym okresie potwierdziła skuteczność EGMS w zwiększaniu precyzji prognozowania ryzyka. Uzyskane wyniki podkreślają potencjał EGMS jako kluczowego narzędzia do systematycznego monitorowania, umożliwiającego wczesne wykrywanie zagrożeń i wzmacniającego bezpieczeństwo miejskie oraz odporność infrastruktury poprzez strategie zapobiegania katastrofom oparte na danych.*

Dane autorów / Authors details:

dr inż. Beata Wieczorek

ORCID 0000-000-9473-2787

beata.zero@uwm.edu.pl

Przesłano / Received 28.10.2024

Zaakceptowano / Accepted 23.12.2024

Opublikowano / Published 31.12.2024



© Submitted for possible open access publication under the terms and conditions of the Creative Commons Attribution (CC BY) license (<http://creativecommons.org/licenses/by/4.0/>).